Valence bond glass — A unified theory of electronic disorder and pseudogap phenomena in high T_c cuprate superconductors

Liang Ren Niestemski and Ziqiang Wang

Department of Physics, Boston College, Chestnut Hill, Massachusetts 02467

We show that the low-energy fluctuations of the valence bond in underdoped high-T_c cuprates, originating from quantum fluctuations of the superexchange interaction, are pinned by the electronic disorder due to off-stoichiometric dopants, leading to a valence bond glass (VBG) pseudogap phase. The antinodal Fermi surface sections are gapped out, giving rise to a normal state Fermi arc whose length shrinks with underdoping. Below T_c, the superexchange interaction induces a d-wave superconducting gap that coexists with the VBG pseudogap. The evolution of the local and momentum-space spectroscopy with doping and temperature captures the salient properties of the pseudogap phenomena and the electronic disorder. The unified theory elucidates the important interplay between strong correlation and the intrinsic electronic disorder in doped transition metal oxides.

The least understood electronic state in the high-T_c cuprates lies in the pseudogap phase that straddles the AF Mott insulator and the d-wave superconductor. The origin of the pseudogap phase is a subject of intensive debate [1]. This unexpected phase is defined by a normal state *pseudogap* in the single-particle excitation spectrum below a characteristic temperature T^* [2, 3]. One of the most intriguing properties is the momentum space anisotropy: the Fermi surface (FS) near the d-wave antinodes is gapped out, leaving a Fermi arc of gapless excitations near the nodes. This nodal-antinodal dichotomy is further enlightened by recent ARPES [4, 5, 6] and Raman [7] experiments that find two distinct spectral gaps in terms of the temperature and doping dependence: a large pseudogap near the antinodes that tracks T^* and a smaller superconducting (SC) gap along the arc that tracks T_c. Recent STM measurements observe a SC gap coexisting spatially with a large pseudogap below T_c [8, 9].

The Fermi arc raises the possibility for an unconventional electronic state. In the absence of disorder, the FS is the trajectory of the poles in the single-particle Green's function (discontinuity in the momentum distribution) and involves continuous contours in momentum space. Thus the Fermi arc must evolve into either a Fermi point or a FS pocket at low temperatures. This difference highlights two different (one-gap and two-gap) proposals for the origin of the pseudogap. In the one-gap scenario, the pseudogap is a d-wave pairing gap without SC phase coherence that evolves into a single SC gap below T_c [1, 10, 11]. The two-gap scenario attributes the pseudogap as due to competing order from an energetically favorable state unrelated to pairing. An important implication of a generic two-gap scenario is the *coexistence* of a d-wave SC gap over the Fermi arc and a low-temperature pseudogap in the antinodal region below T_c [12]. The observation of two distinct gaps by ARPES, Raman, and STM experiments provides strong support for the two-gap scenario.

A consistent theory for the pseudogap has been challenging. Most of the proposals for a competing state invoke various density waves and flux/orbital current order [1, 10] that break translation symmetry by one lattice constant and result in superstructures. The FS is truncated in the antinodal region by band-folding with respect to a unique ordering wavevector q, leading to FS pockets and particle-hole asymmetric pseudogap density of states [13]. However, despite many years of effort and the much improved measurement resolution, no signatures of disguised FS pockets or folded bands have been detected in zero external fields.

A related phenomenon in the cuprates is the electronic disorder. There has been mounting STM evidence for nanoscale DOS gap disorder [14, 15, 16, 17, 18] and, under a variety of conditions where superconductivity is weakened, short-range ordered checkerboard DOS modulations [15, 18, 19, 20] which are manifestations of a bond-centered electronic glass [21]. A natural cause for the electronic disorder is the out of plane ionic dopants, interstitial in $Bi_2Sr_2CaCu_2O_{8+x}$, substitutional in $La_{2-x}Sr_xCuO_4$ and $Ca_{2-x}Na_xCuO_2Cl_2$, and in combination with chemical substitutions in $Bi_2Ln_{2-z}Bi_zCuO_{6+x}$ (Ln-Bi2201). In addition to inducing structural distortions, the screening of the dopant electrostatic potential is highly nonlinear in doped Mott insulators due to strong Coulomb repulsion, leading to inhomogeneous electronic states with spatial variations in the local doping concentration [22, 23].

We present here a unified theory for the pseudogap phenomena and the electronic disorder. The key point is the interplay between strong correlation induced valence bond fluctuations and the dopant induced disorder. In the parent compounds, the superexchange interaction between the Cu spins, described by the nearest neighbor Heisenberg model $H_J = J \sum_{\langle i,j \rangle} \mathbf{S}_i \cdot \mathbf{S}_j$, causes AF order in the ground state. Due to strong quantum fluctuations of the spin-1/2 moment, the nonmagnetic *valence bond states* are close in energy to the AF state. Writing $\mathbf{S}_i \cdot \mathbf{S}_j = \frac{1}{2} c^\dagger_{i\sigma} c_{i\sigma'} c^\dagger_{j\sigma'} c_{j\sigma} + \text{const.}$, the valence bond can be formed via spin-singlet pairing $\Delta_{ij} = \langle c_{i\uparrow} c_{j\downarrow} - c_{i\downarrow} c_{j\uparrow} \rangle$ as in the resonance valence bond (RVB) theory [24], and the paramagnetic $\chi_{ij} = \sum_\sigma \langle c^\dagger_{i\sigma} c_{j\sigma} \rangle$ as envisioned by Pauling in chemical bonding. Since charge fluctuations are completely suppressed, the two descriptions are equivalent and the valence bond states are highly degenerate owing to the SU(2) symmetry [25]. Besides valence bond liquid states, there are also symmetry breaking valence bond crystal states that are gapped but competitive in energy [1, 26]. Doping the Mott insulator breaks the SU(2) symmetry and makes the valence

bond in the particle-particle and particle-hole channels different. The basic question is which fluctuating valence bond state is selected when a sufficient amount of holes destroys the AF long-range order. In the short-range RVB theory, the spin-singlet pairs are mobilized by the doped holes and condense into a d-wave SC state [27]. There is, however, a natural competing order driven by the same superexchange interaction, i.e. the paramagnetic valence bond χ_{ij}.

We show that the d-wave component of the *real part* of χ_{ij} represents the most important low-energy fluctuations and that dopant induced disorder pins such d-wave charge density wave fluctuations to an electronic valence bond glass (VBG) phase exhibiting the observed pseudogap phenomena. This is similar in spirit to disorder induced glassy phases or the nematic liquid crystal of stripes [28, 29]. A ubiquitous feature of the VBG is the emergence of a pseudogap near the antinodes where the valence bond fluctuations are large due to the flatness of the band, giving rise to a genuine normal state Fermi arc. Based on microscopic calculations of the extended t-J model using spatially unrestricted Gutzwiller approximation, we show that the VBG captures the salient properties of the observed pseudogap phenomena and electronic disorder, especially in underdoped and chemically substituted bilayer and single-layer Bi-based cuprates where the pseudogap and the SC gap are well separated [4, 5, 6, 8, 9].

The Hamiltonian of the extended t-J model is given by

$$H = -\sum_{i \neq j} t_{ij} P_i c_{i\sigma}^\dagger c_{j\sigma} P_j + J \sum_{\langle i,j \rangle} \left(\mathbf{S_i} \cdot \mathbf{S_j} - \frac{1}{4} \hat{n}_i \hat{n}_j \right) + \sum_i V_i \hat{n}_i. \quad (1)$$

The electrons hop between near neighbors via t_{ij}. Repeated spin indices are summed, $\hat{n}_i = c_{i\sigma}^\dagger c_{i\sigma}$, $\mathbf{S}_i = \frac{1}{2} c_{i\sigma}^\dagger \tau_{\sigma\sigma'} c_{i\sigma'}$. The projection operator P_i removes double occupation on site-i. The last term in Eq. (1) is the electrostatic potential, $V(i) = \sum_{j \neq i} \frac{V_c}{|r_i - r_j|} (n_j - \bar{n}) + \sum_{\ell=1}^{N_d} \frac{V_d}{\sqrt{|r_i - r_\ell|^2 + d_s^2}}$, where the long-range Coulomb interaction of strength V_c between the in-plane electrons provides the important screening of the ionic potential of strength V_d from N_d number of off-plane dopants at a set back distance d_s [22, 23]. We use $J = 120$meV and up to fifth nearest neighbor hoppings $t = (360, -120, 29, 24, -24)$meV relevant for the band structure [30] and set $V_c = V_d = 0.5$eV and $d_s = 1$ in units of the lattice constant [22]. To account for their Coulomb repulsion, the ionized dopant configurations are generated randomly with a hard-core of one to three lattice spacings.

To account for both strong correlation and disorder, we use the spatially unrestricted Gutzwiller projected wave function $|\Psi\rangle = \prod_i y_i^{\hat{n}_i} (1 - \hat{n}_{i\uparrow} \hat{n}_{i\downarrow}) |\Psi_0\rangle$, where Ψ_0 is a Slater determinant state and y_i is a *local* fugacity that keeps the density unchanged before and after projection. The projection is implemented using the Gutzwiller approximation [31, 32]. The t-J Hamiltonian is replaced by one in the unprojected space with renormalized hopping and exchange that capture the basic Mott physics: $t_{ij} \to g_{ij}^t t_{ij}$ and $J \to g_{ij}^J J$. In an inhomogeneous state, $g_{ij}^t = \sqrt{4 x_i x_j / (1 + x_i)(1 + x_j)}$, $g_{ij}^J = 4/(1 + x_i)(1 + x_j)$
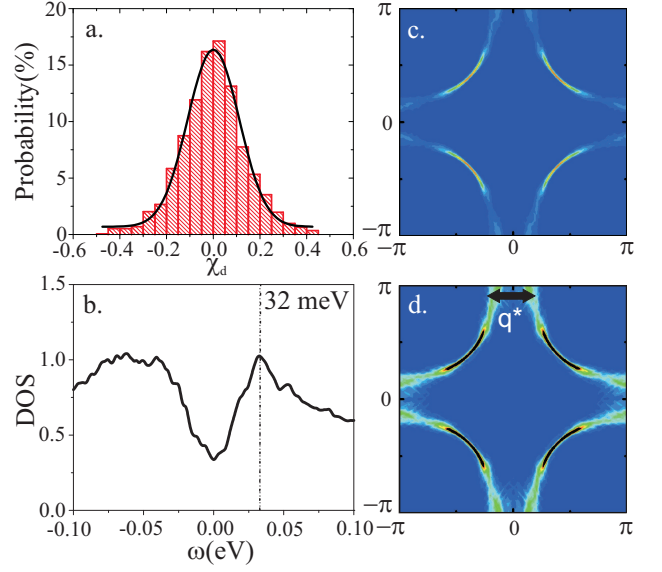

Figure 1: Normal state pseudogap and Fermi arc at $x = 0.125$. (a) Distribution of d-wave valence bond showing glassy order. (b) Averaged DOS showing VBG pseudogap. (c) and (d) Fermi arc.

depend on the *local doping* x_i [13, 23]. Decoupling the exchange interaction in terms of the valence bond χ_{ij} and singlet pairing Δ_{ij}, we obtain a Gutzwiller renormalized Hamiltonian,

$$\begin{aligned} H_{\text{GA}} = & -\sum_{i \neq j} g_{ij}^t t_{ij} c_{i\sigma}^\dagger c_{j\sigma} + \sum_i (V_i + \lambda_i) c_{i\sigma}^\dagger c_{i\sigma} - \sum_i \lambda_i n_i \\ & - \frac{1}{4} J \sum_{\langle i,j \rangle} g_{ij}^\chi \left(\chi_{ij}^* c_{i\sigma}^\dagger c_{j\sigma} + \text{h.c.} - |\chi_{ij}|^2 \right) \\ & - \frac{1}{4} J \sum_{\langle i,j \rangle} g_{ij}^\Delta \left(\Delta_{ij}^* \varepsilon_{\sigma\sigma'} c_{i\sigma} c_{j\sigma'} + \text{h.c.} - |\Delta_{ij}|^2 \right), \quad (2) \end{aligned}$$

where $g_{ij}^\chi = g_{ij}^\Delta = g_{ij}^J$ and λ_i originates from the local fugacity. We minimize the ground state energy of Eq. (2) through self-consistently determined $\{x_i, \lambda_i, \chi_{ij}, \Delta_{ij}\}$ on 24×24 systems for different dopant configurations.

Normal state VBG pseudogap phase. In the normal state above T_c or the zero temperature phase with $\Delta_{ij} = 0$, we find that the valence bond χ_{ij} is *real* and fluctuates due to the disorder potential in the doping range studied. The dominant fluctuation is in the d-wave channel, $\chi_d(i) = \frac{1}{4} \sum_j d_{ij} \chi_{ij}$, with the form factor $d_{ij} = \pm 1$ for the four bonds emanating from site i. We first focus on the normal state by setting $\Delta_{ij} = 0$. The histogram of χ_d at average doping $x = 0.125$ is shown in Fig. 1a. It follows a Gaussian distribution with zero mean. The root-mean-squared fluctuation represents a nonzero "glassy" order parameter $\delta_\chi = \sqrt{\sum_i \chi_d^2(i)/N_s} = 0.28$ for the VBG phase. We note that glassy dynamics of valence bond was studied in the weak-coupling metallic phase of the Hubbard-Heisenberg model at half-filling [33]. The most succinct feature of the VBG is the emergence of the pseudogap and the Fermi arc. The averaged DOS in Fig. 1b shows a remarkable V-shaped pseudogap, $\Delta_{pg} \sim 32$meV, approximately symmetrically dis-
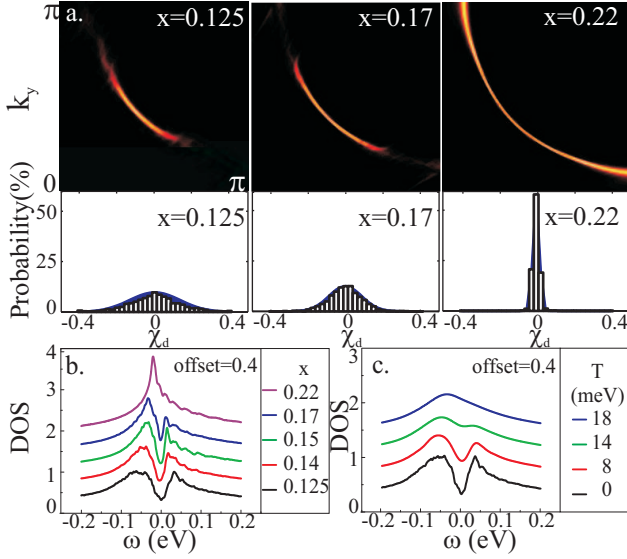
Figure 2: Doping dependence of the Fermi arc and valence bond glassy order (a) and averaged DOS and pseudogap (b). (c) Temperature evolution of VBG pseudogap at $x = 0.125$.

Figure 3: Angle dependence of symmetrized spectral function (a) and pseudogap (b). (c) Doping dependence of pseudogap from DOS (circles) and d-wave valence bond order parameter (squares). (d) $|\chi_d(q)|$ along q_x-direction with peaks at q^* marked in Fig. 1d.

tributed around the Fermi level due to the d-wave nature of the VBG. The calculated spectral intensity at the Fermi energy in Fig. 1c reveals a FS truncated near the antinodes by the pseudogap and a Fermi arc around the nodes. The Fermi arc tracks the underlying FS and remains prominent upon lowering the intensity scale in Fig. 1d without signs of band folding.

The doping and temperature dependence of the VBG pseudogap is shown in Fig. 2. With increasing doping, the distribution of the valence bond in Fig. 2a sharpens around zero, the VBG order parameter δ_χ reduces, and the Fermi arc length increases in agreement with ARPES experiments. Note that while the density of off-plane dopants increases with doping, δ_χ decreases due to improved screening by more mobile carriers that leads to weaker fluctuations of the potential V_i. The doping evolution of the averaged DOS is shown in Fig. 2b. The pseudogap becomes smaller and shallower with increasing doping and becomes undiscernible beyond $x = 0.22$ on the shoulder of the van Hove peak. The extracted pseudogap has a doping dependence that follows $\Delta_{pg} \simeq (J/8)\sqrt{\sum_i(\sum_j g^\chi_{ij}\chi_{ij}d_{ij})^2/N_s}$, as shown in Fig. 3c. The temperature evolution of the pseudogap obtained by minimizing the free energy of Eq. (2) is shown in Fig. 2c at $x = 0.125$. The pseudogap onset temperature $T^* \simeq 16$meV is clearly seen to be determined by the thermal filling of the VBG pseudogap.

The momentum-dependence of the symmetrized spectral function $A(k,\omega)$ is plotted in Fig. 3a at Fermi level for $x = 0.14$. It shows gapless quasiparticle excitations along the arc and the opening of the pseudogap at the arc tip that increases toward the antinode. The angular dependence of the pseudogap extracted this way is shown in Fig. 3b. Away from the zero-gap Fermi arc regime, the pseudogap follows the d-wave form (dashed line) consistent with the d-wave nature of the
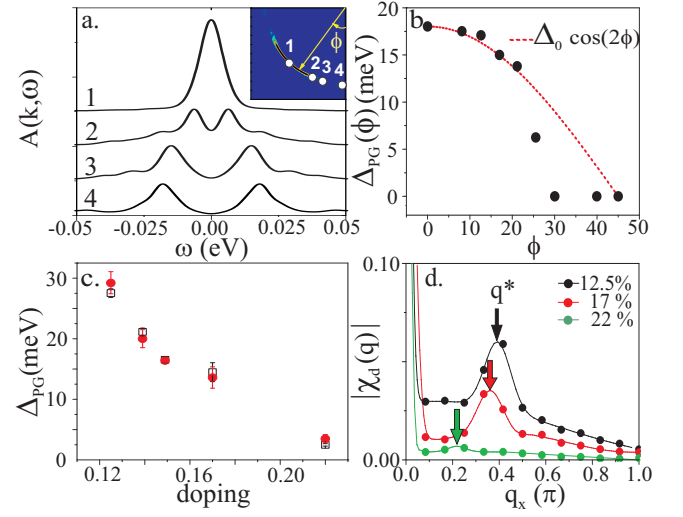
VBG. The line-shape in Fig. 3a shows that the pseudogap near the antinodes is a *soft gap*. This important prediction of the VBG is consistent with the original ARPES experiments [2, 3] and differs from the naive picture of a hard gap that depletes all states near the antinode below the pseudogap energy scale. These in-gap states contribute to the spectral weight at low energy and have important consequences in the SC state.

The pseudogap in the VBG theory is not sensitive to the precise topology of the FS and does not require the antinodal FS sections to be parallel which can induce long-range incommensurate density wave order [13]. We obtain similar results using a different set of hopping parameters $t = (480, -160, 50, 50, -50)$meV used in Ref.[23] that does not favor the antinodal nesting condition. A band dispersion showing the observed flatness near the antinode suffices. The propensity toward the VBG is due to an enhanced static susceptibility broadly peaked around the q^* shown in Fig. 1 that enables electronic disorder to pin the VBG with a distribution of $\chi_d(q)$ peaked around q^*. In Fig. 3d, we show the Fourier power spectrum $|\chi_d(q)|$ plotted along the q_x-direction. Both the peak and the incommensurate q^* decrease with increasing doping. At $x = 0.14$, $q^* \simeq (\pm 0.4\pi, 0)$, indicative of glassy $\sim 5 \times 5$ checkerboard patterns for the valence bond.

Superconducting phase. The VBG can coexist with an inhomogeneous d-wave superconductor; both due to the superexchange interaction. Although the Gutzwiller factors $g^\chi_{ij} = g^\Delta_{ij}$, charge fluctuations at finite doping, and in particular, the pair-breaking induced by inter-site Coulomb repulsion will weaken the singlet pairing channel [34]. Moreover, the electron-phonon interactions have been shown to promote the d-wave charge density wave [35, 36]. To incorporate these effects into the renormalized mean field theory in Eq. (2), we use $g^\chi_{ij} = g^J_{ij}$ and $g^\Delta_{ij} = pg^J_{ij}$ with $p = 0.475$, which separates
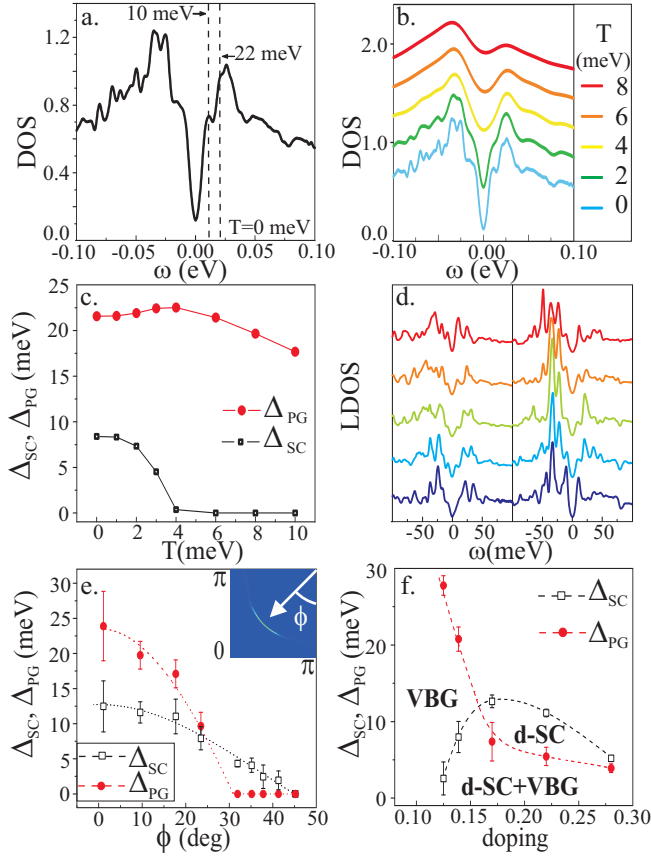
Figure 4: SC state at $x = 0.14$. (a) and (b) Averaged DOS showing SC gap and VBG pseudogap. (c) Temperature dependence of Δ_{sc} and Δ_{pg}. (d) LDOS along two line cuts. (e) Angular dependence of SC gap and pseudogap. (f) Δ_{sc} and Δ_{pg} as a function of doping.

discussed above which allows pairing of the antinodal states inside the pseudogap. The ground state below T_c is thus a coherent mixture of d-wave VBG and SC pairs; there are traits of the glassy valence bond order in the pairing gap near the antinode and *vice versa*. Although incoherent background and inelastic life-time broadening tend to mask the coherent peak and the pairing gap near the antinode in the spectral function, recent high resolution ARPES experiments on La-Bi2201 indeed observe two gaps near the antinodes [9, 37].

In summary, we presented a VBG theory for the essential features of the normal state pseudogap and the two-gap phenomena in the SC state. In Fig. 4f, we construct a theoretical phase diagram using the doping dependence of the d-wave pairing gap and the VBG pseudogap. It captures the basic topology of the global phase diagram of the high-T_c cuprates. Although the present theory does not include a precursor pairing induced pseudogap above T_c, it does not rule out such a possibility due to fluctuations beyond the Gutzwiller theory.

the two energy gap scales in the underdoped regime. The averaged DOS at $T = 0$ is shown in Fig. 4a for $x = 0.14$. It displays two gaps: a smaller SC gap $\Delta_{sc} \simeq 10$meV and a large pseudogap $\Delta_{pg} \simeq 22$meV inherited from the normal state, in agreement with STM experiments on La-Bi2201 [8, 9]. The temperature evolution in Fig. 4b shows that the SC gap and coherence peaks disappears above $T_c \sim 4$meV as the system enters the pseudogap phase. Interestingly, as T is increased toward T_c, the pairing gap and the pseudogap show opposite temperature dependence (Fig. 4c), a typical feature of coexisting but competing order.

In Figs. 4d, the local DOS (LDOS) is shown along two line cuts on a typical sample at $x = 0.14$. The evolution of the line-shape agrees with the STM conductance spectra observed in La-Bi2201 [8, 9], exhibiting two coexisting low energy gaps that are spatially inhomogeneous. The momentum dependence of the two gaps, calculated from the single-particle spectral function $A(k, \omega)$, is plotted along the underlying FS in Fig. 4e. Remarkably, the d-wave pairing gap extends beyond the Fermi arc into the antinodal regime. The coexistence of the two gaps off the Fermi arc in momentum space is an important prediction of the present theory. Physically, this is a consequence of the softness of the normal state pseudogap

[1] P.A. Lee et al., Rev. Mod. Phys. **78**, 17 (2006).
[2] A.G. Loeser et al., Science **273**, 325 (1996).
[3] H. Ding et al., Nature **382**, 51 (1996).
[4] K. Tanaka et al., Science **314**, 1910 (2006).
[5] W.S. Lee et al., Nature, **450**, 81 (2007).
[6] T. Kondo et al., Phys. Rev. Lett. **98**, 267004 (2007).
[7] M. Le Tacon et al., Nature Phys. **2**, 537 (2006).
[8] M. C. Boyer et al., Nature Phys. **3**, 802 (2007); W.D. Wise et al., arXiv:0806.0203.
[9] J.-H. Ma, et al., Phys. Rev. Lett. **101**, 207002 (2008).
[10] M.R. Norman, et al., Phys. Rev. B**76**, 174501 (2007).
[11] A. Kanigel et al., Phys. Rev. Lett. **99**, 157001 (2007).
[12] M. Civelli et al., Phys. Rev. Lett. **100**, 046402 (2008).
[13] C. Li et al., Phys. Rev. B**73**, 060501 (2006).
[14] S.H. Pan et al., Nature **413**, 282 (2001).
[15] C. Howald et al., Phys. Rev. B**64**, 100504 (2001).
[16] K.M. Lang et al., Nature **415**, 412 (2002).
[17] K. McElroy et al., Science **309**, 1048 (2005).
[18] T. Hanaguri et. al. Nature **430**, 1001 (2004).
[19] M. Vershinin et al., Science **303**, 1995 (2004).
[20] K. McElroy et al. Phys. Rev. Lett. **94**, 197005 (2005).
[21] Y. Kohsaka et al., Science **315**, 1380 (2007).
[22] Z. Wang et. al. Phys. Rev. B**65**, 064509 (2002).
[23] S. Zhou et al., Phys. Rev. Lett. **98**, 076401 (2007).
[24] P.W. Anderson, Science **235**, 1196 (1987).
[25] I. Affleck, *et. al.*, Phys. Rev. B**38**, 745 (1988).
[26] D. Rokhsar, S.A. Kivelson, Phys. Rev. Lett. **61**, 2376 (1988).
[27] P.W. Anderson et al., J. Phys. Cond. Matt. **16** R755 (2004).
[28] S.A. Kivelson et al., Rev. Mod. Phys. **75**, 1201 (2003).
[29] M. Vojta, Phys. Rev. B**78**, 144508 (2008).
[30] M.R. Norman and H. Ding, Phys. Rev. B**57**, 11089 (1998).
[31] D. Vallhardt, Rev. Mod. Phys. **56**, 99 (1984).
[32] F.C. Zhang, et al., Supercond. Sci. Technol. **1**, 36 (1988).
[33] M. Tarzia and G. Biroli, Europhys. Lett. **82**, 67008 (2008).
[34] S. Zhou and Z. Wang, Phys. Rev. B**70**, 020501 (2004).

[35] D.M. Newns and C.C. Tsuei, Nature Phys. **3**, 184 (2007).

[36] J.-X. Li et al., Phys. Rev. B**74**, 184515 (2006).

[37] J. Wei et al., Phys. Rev. Lett. **101**, 097005 (2008).